PCCP

Accepted Manuscript

ROYAL SOCIETY OF CHEMISTRY

www.rsc.org/pccp

Beyond the molecular orbital conception of electronically excited states through the quantum theory of atoms in molecules

David Ferro-Costas [1], Ángel Martín Pendás [2], Leticia González [3], and Ricardo A. Mosquera*[1]

[1]Departamento de Química Física, Universidade de Vigo, Facultade de Química, Lagoas-Marcosende s/n, 36310 Vigo, Spain
[2]Departamento de Química Física y Analítica, Facultad de Química, Universidad de Oviedo, 33006-Oviedo, Spain
[3]Institute of Theoretical Chemistry, University of Vienna, Währinger Str. 17, 1090 Vienna, Austria

Abstract

We show that the use of the quantum theory of atoms in molecules (QTAIM) in electronically excited states allows expanding the knowledge that the molecular orbital (MO) framework provides about electronic rearrangements. Despite historical prejudices seemed to preclude the use of QTAIM beyond the electronic ground state, this paper evidences that QTAIM is versatile enough to deal with excited states. As an example, the paradigmatic $n \rightarrow \pi^*$ electronic transition for formaldehyde is analyzed. Using QTAIM, an energy partition of excited state energies into atomic and diatomic energies is carried out for the first time. This partition shows that upon electronic excitation the atoms of the CO bond experience a stabilization in their net energies, accompanied by a destabilization in their interaction, fact which is in accordance with the idea of populating an antibonding π^* MO. The associated C−O elongation in the $n\pi^*$ state does not involve a change in the π atomic populations –as one would expect from a π^* orbital– but in the σ ones. Moreover, it is also found that the $n\pi^*$ state is characterized by a weaker C−O interaction energy in comparison to that in the electronic ground state. In order to strengthen this interaction, the electron-electron repulsion between C and O is reduced via a symmetry-breaking of the electron density, causing the C pyramidalization. A topological analysis based on the Laplacian of the electron density and on the electron localization function (ELF) reveals that the $n \rightarrow \pi^*$ transition can be visualized as a rotation of 90° of the oxygen lone pairs.

Keywords: Formaldehyde, electronic excited states, QTAIM, IQA scheme, nπ^* states, ELF, electronic structure theory.

*Email: mosquera@uvigo.es; Corresponding author

1 Introduction

Understanding the nature of electronically excited states is fundamental in disciplines ranging from basic synthetic organic and inorganic chemistry to nanotechnology and biology. Photoinduced processes are basic to life itself through photosynthesis, and it has become increasingly clear that many biologically important molecules have been subjected to strong natural selection favoring their photostability.[1] A theoretical approach to these problems has traditionally been hindered due to difficulties in solving the time-independent Schrödinger equation for states different from the ground state. However, computational advances in the last decade are starting to revert the situation and, with the introduction of multireference methods and the developments on linear scaling techniques,[2] *ab initio* predictability in excited states for moderately sized systems can be reached.[3]

Conspicuously, despite the increasing wide black-box availability of computational methods to aid practicing chemists, most experiments are designed and/or interpreted in terms of a set of rules that were introduced to understand chemical bonding in electronic ground states. Some of these rules are based on the one-electron approximation inherent to one determinant descriptions as, for example, the use molecular orbital (MO) arguments to understand reactivity pathways. Unfortunately, this approximation is sometimes poor, specially in the case of electronic excited states. It is for this reason that a working framework to understand chemical bonding in excited states still needs to be appropriately developed.

Any chemical bonding paradigm for excited states must be able to tackle multireference systems and, as a consequence, it cannot rely on a fixed set of one electron functions (orbitals). Mainstream ground state chemical bonding theory is still dominated by MO thinking (an intrinsically one-electron scheme). As such, more than often, it offers results strongly dependent on the method used to obtain the approximated wave function because MOs are not invariant under orbital transformations. One textbook example is the description of the double C=C bond in ethylene. While the Pipek-Mezey localization method[4] provides a representation based on one σ MO and one π orbital, the Boys localization method[5,6] describes the bond by two equivalent banana bond orbitals. Such a situation could be, in a certain way, confused for some practicing chemists. A possible way out to this ambivalence is to rewrite chemical bonding theory in terms of orbital invariant quantities. These objects can be obtained in terms of reduced density matrices (RDMs), either in position or momentum space. As the chemist's language is developed in the physical space, most of the implementations proposed so far are based on $\mathbf{r}$ dependent RDMs, and these methods are collectively known as real space theories

of chemical bonding.

RDMs depend on spin-spatial coordinates and lack atomic information intrinsic to orbitals. Fortunately, Richard F. W. Bader paved this road by showing how atomic, and in general, chemically meaningful regions may be extracted from the RDMs[7,8] by examining the topology induced by the electron density, ρ. This, so-called Quantum Theory of Atoms in Molecules (QTAIM), has provided deep insights into the nature of the chemical bond for over thirty years, and its methods have been widely generalized to develop what is called Quantum Chemical Topology (QCT).[9] QTAIM thinking satisfies all of the requirements previously commented: it is invariant under orbital transformations, all of its descriptors are equally defined and obtained for one determinant or correlated wave functions (thus providing an smooth procedure to understand how correlation affects bonding), and it includes an exact energy partitioning into atomic and interatomic contributions.[10]

Traditionally, the QTAIM is thought of as a theory of ground state molecules. This historical prejudice roots to the difficulties of the topological procedure to properly define atoms in simple excited states, like the $2s$ H atom, for which each attraction basin of ρ, i.e. each of its local maxima, defines a quantum atom in the theory. A similar situation is found in the ground state of some molecules, e.g. in Li_2, which displays a non-nuclear maximum of the electron density at the internuclear midpoint.[11] However, the controversy on ground state non-nuclear maxima is now over, their existence related to important concepts like F-centers in ionic solids.[12] Despite a large class of chemically important molecules do not show excited states with non-nuclear attractors, the use of QTAIM to aid understanding excited state processes is scarce.[13–17]

To our knowledge, this paper is the first in performing an energetic partition scheme based on QTAIM regions that allows to understand physically the evolution of the charge density and geometry of a molecule upon excitation. This type of analysis can be extremely helpful to explain, in an orbital invariant language, photophysical and photochemical phenomena. As a practical example, a paradigmatic process in photochemistry, the $n \rightarrow \pi^*$ electronic transition, has been selected. A simple but very well studied molecule, formaldehyde, is chosen to illustrate how QTAIM can explain the molecular changes that take place after the electronic excitation. Three electronic states will be analyzed: the ground S_0 and the first singlet S_1 and triplet T_1 states. In the traditional MO language, S_1 and T_1 are understood as one-electron excitations from a non-bonding MO centered at the oxygen atom (the n lone pair) to the C−O antibonding π^* orbital. According to textbook MO machinery, populating the π^* MO weakens the C−O double bond and this manifests as a lengthening of the bond. Concurrently, the hybridization of the C atom changes from sp^2-like to sp^3 leading to a C pyramidalization in any of the two

S_1 and T_1 excited states.[18] In this work we shall show the ability of the QTAIM to cope with excited states and we will carefully monitor the QTAIM interpretation against the traditional MO explanation, to correlate both views as much as possible.

2 Methodology

2.1 Basic descriptors of the quantum theory of atoms in molecules

Bader and coworkers showed that the topology induced by the electron density, $\rho(\mathbf{r})$, comes from generalizing the quantum mechanics to subsystems in $\mathbb{R}^3$. These subsystems (Ω) are associated to the atoms in the molecule and they are referred as "atomic basins". In the following, the QTAIM descriptors employed in this paper are briefly revised. Further information can be found in Refs.[7,8,19].

Some elements of chemical structure can be identified with critical points of $\rho(\mathbf{r})$. For example, critical points exhibiting three negative curvatures are called nuclear critical point (NCPs), as they are normally placed at, or close to, the position of the nuclei. Critical points with two negative curvatures (and one positive) are called bond critical points (BCPs). The line of locally maximum density linking two NCPs define what is known as bond path and its presence implies that the corresponding atoms are bonded to one another. The interaction between a given pair of atoms bonded is characterized according to the properties of the electron and energy densities at the BCP.

Two interesting descriptors are defined at the BCP. One is the electron density at that point, ρ^{BCP}, and it is related to the strength of the bonding. The second is the ellipticity, ϵ, which measures the extent to which density is preferentially accumulated in a given plane containing the bond path, and it is defined as follows

$$\epsilon^{BCP} = \frac{\lambda_1}{\lambda_2} - 1, \quad \text{with} \quad |\lambda_1| \geqslant |\lambda_2| \tag{1}$$

and where λ_1 and λ_2 are the eigenvalues of the Hessian matrix associated to the eigenvectors which form a plane perpendicular to the bond path. If $\lambda_1 = \lambda_2$ then $\epsilon = 0$ and the bond is cylindrically symmetrical –situation that can be found e.g. at the C−C bonds of ethane and ethine. As such, ϵ^{BCP} has been related to the π character, providing reasonable results for most of single and double bonds between carbons.

The average number of electrons associated to the atomic basin Ω, $N(\Omega)$, can be obtained

by

$$N(\Omega) = \int_{\Omega} \rho(\mathbf{r}) d\mathbf{r} \tag{2}$$

These atomic electron populations are usually transformed into net atomic charges by

$$q(\Omega) = Z - N(\Omega) \tag{3}$$

where Z is the nuclear charge of the corresponding atom. Moreover, it can be shown that $N(\Omega)$ can be split into two kind of terms:

$$N(\Omega) = \lambda_{\Omega} + \frac{1}{2} \sum_{\Omega' \neq \Omega} \delta_{\Omega,\Omega'} \tag{4}$$

The term λ_{Ω} is associated exclusively to Ω and is called localization index. The terms related to pair of basins, $\delta_{\Omega,\Omega'}$, are called delocalization indices and measure the number of electrons shared between Ω and Ω'.

2.2 Energy partition

Within the Born-Oppenheimer approximation, the expected value for the molecular electronic energy, E, is given by:

$$E = \langle \Psi | \widehat{H} | \Psi \rangle = T + V_{ne} + V_{ee} + V_{nn} \tag{5}$$

where $\widehat{H}$ is the Hamiltonian of the system, T is the kinetic energy, V_{ne} is the nucleus-electron attraction, and V_{ee} and V_{nn} are, respectively, the electron-electron and the nucleus-nucleus repulsions.

All these quantities can be written in terms of the electron density of the system, $\rho(\mathbf{r})$:

$$V_{ne} = -\sum_{\alpha=1}^{M} \int \frac{Z_{\alpha} \rho(\mathbf{r})}{|\mathbf{R}_{\alpha} - \mathbf{r}|} d\mathbf{r} \tag{6}$$

$$V_{coul} = \frac{1}{2} \int \frac{\rho(\mathbf{r}_1)\rho(\mathbf{r}_2)}{|\mathbf{r}_2 - \mathbf{r}_1|} d\mathbf{r}_1 d\mathbf{r}_2 \tag{7}$$

the spin-free first order RDM, $\gamma(\mathbf{r}, \mathbf{r}')$:

$$T = -\frac{1}{2} \int_{\mathbf{r}' \to \mathbf{r}} \nabla^2 \gamma(\mathbf{r}, \mathbf{r}') d\mathbf{r} \tag{8}$$

and the exchange-correlation component of the diagonal second order RDM, $\Gamma_{xc}(\mathbf{r}_1, \mathbf{r}_2)$:

$$V_{xc} = \frac{1}{2} \int \frac{\Gamma_{xc}(\mathbf{r}_1, \mathbf{r}_2)}{|\mathbf{r}_2 - \mathbf{r}_1|} d\mathbf{r}_1 d\mathbf{r}_2 \tag{9}$$

where $\mathbf{r}$, $\mathbf{r}_1$ and $\mathbf{r}_2$ represent electron coordinates; M is the number of nuclei; and Z_α and $\mathbf{R}_\alpha$ are the charge and the position vector of the α nucleus. The total electron-electron repulsion, V_{ee}, is split into a classic Coulomb term (V_{coul}, eq 7) and another associated to the exchange-correlation of the system (V_{xc}, eq 9):

$$V_{ee} = V_{coul} + V_{xc} \tag{10}$$

As QTAIM provides a partition of the three-dimensional space into atomic basins, the electron density is also susceptible of partition into atomic contributions:

$$\rho(\mathbf{r}) = \sum_{\Omega} \rho_\Omega(\mathbf{r}) = \sum_{\Omega} w_\Omega(\mathbf{r})\rho(\mathbf{r}) \tag{11}$$

where Ω represents an atomic basin and the function w_Ω is defined, for the QTAIM partition, by

$$w_\Omega(\mathbf{r}) = \begin{cases} 1 & \text{if} \quad \mathbf{r} \in \Omega \\ 0 & \text{elsewhere} \end{cases} \tag{12}$$

Likewise, the RDMs can be also partitioned as

$$\gamma(\mathbf{r}, \mathbf{r}') = \gamma(\mathbf{r}, \mathbf{r}') \sum_{\Omega} w_\Omega(\mathbf{r}') = \sum_{\Omega} \gamma_\Omega(\mathbf{r}, \mathbf{r}') \tag{13}$$

$$\Gamma_{xc}(\mathbf{r}_1, \mathbf{r}_2) = \sum_{\Omega}\sum_{\Omega'} w_\Omega(\mathbf{r}_1) w_{\Omega'}(\mathbf{r}_2) \Gamma_{xc}(\mathbf{r}_1, \mathbf{r}_2) = \sum_{\Omega}\sum_{\Omega'} \Gamma_{xc}^{\Omega\Omega'}(\mathbf{r}_1, \mathbf{r}_2) \tag{14}$$

allowing for a whole division of the molecular energy into atomic and diatomic terms.[10] For instance, using eq 13 in 8, we obtain:

$$T = \sum_{\Omega} -\frac{1}{2} \int_{\mathbf{r}' \to \mathbf{r}} \nabla^2 \gamma(\mathbf{r}, \mathbf{r}') w_\Omega(\mathbf{r}') d\mathbf{r} = \sum_{\Omega} T(\Omega) \tag{15}$$

Similarly, through eq 11, V_{ne} is given by

$$V_{ne} = \sum_{\Omega}\sum_{\alpha=1}^{M} \int_\Omega \frac{-Z_\alpha \rho(\mathbf{r})}{|\mathbf{R}_\alpha - \mathbf{r}|} d\mathbf{r} = \sum_{\Omega}\sum_{\alpha=1}^{M} V_{ne}(\alpha, \Omega) \tag{16}$$

Finally, the electron-electron repulsion results in:

$$V_{ee} = \sum_{\Omega} \underbrace{\{V_{coul}(\Omega, \Omega) + V_{xc}(\Omega, \Omega)\}}_{V_{ee}(\Omega,\Omega)} + \frac{1}{2} \sum_{\Omega} \sum_{\Omega' \neq \Omega} \underbrace{\{V_{coul}(\Omega, \Omega') + V_{xc}(\Omega, \Omega')\}}_{V_{ee}(\Omega,\Omega')} \tag{17}$$

where the Coulomb components are:

$$V_{coul}(\Omega, \Omega) = \frac{1}{2} \int_\Omega \int_\Omega \frac{\rho(\mathbf{r}_1)\rho(\mathbf{r}_2)}{|\mathbf{r}_2 - \mathbf{r}_1|} d\mathbf{r}_1 d\mathbf{r}_2 \tag{18}$$

$$V_{coul}(\Omega,\Omega') = \int_{\Omega}\int_{\Omega'} \frac{\rho(\mathbf{r}_1)\rho(\mathbf{r}_2)}{|\mathbf{r}_2-\mathbf{r}_1|} d\mathbf{r}_1 d\mathbf{r}_2 \tag{19}$$

and the exchange-correlation:

$$V_{xc}(\Omega,\Omega) = \frac{1}{2}\int_{\Omega}\int_{\Omega} \frac{\Gamma_{xc}(\mathbf{r}_1,\mathbf{r}_2)}{|\mathbf{r}_2-\mathbf{r}_1|} d\mathbf{r}_1 d\mathbf{r}_2 \tag{20}$$

$$V_{xc}(\Omega,\Omega') = \int_{\Omega}\int_{\Omega'} \frac{\Gamma_{xc}(\mathbf{r}_1,\mathbf{r}_2)}{|\mathbf{r}_2-\mathbf{r}_1|} d\mathbf{r}_1 d\mathbf{r}_2 \tag{21}$$

Once the partition of all the energetic terms associated with the operators comprising the Hamiltonian of the system is done, different terms can be grouped. The collection of all the terms that takes place exclusively in one atomic basin results in the definition of the net energy for that atom, E_{net},

$$E_{net}(\Omega) = T(\Omega) + V_{ne}(\omega,\Omega) + V_{ee}(\Omega,\Omega) \tag{22}$$

where ω represents the nucleus that belongs to the Ω basin. Similarly, the interaction energy (V_{int}) between 2 atoms can be defined according

$$V_{int}(\Omega,\Omega') = V_{nn}(\omega,\omega') + V_{ne}(\omega,\Omega') + V_{ne}(\omega',\Omega) + V_{ee}(\Omega,\Omega') \tag{23}$$

for $\Omega \neq \Omega'$ and $\omega \neq \omega'$. The introduction of both kind of energies (net and interaction) in eq 5 yields the chief equation of the interacting quantum atoms (IQA) energy partition scheme:

$$E = \sum_{\Omega} E_{net}(\Omega) + \frac{1}{2}\sum_{\Omega}\sum_{\Omega'\neq\Omega} V_{int}(\Omega,\Omega') \tag{24}$$

According to this equation, a molecular system can be analysed in terms of its constituent elements (atoms or even group of them) and their interactions. This point of view resembles the traditional conception of chemistry before the introduction of quantum mechanics and it does not invoke orbital definitions.

2.3 Computational Details

All the geometries have been optimized using the Complete Active Space Self Consistent Field (CASSCF) procedure[20] with an active space of 12 electrons distributed in 10 MOs. The active space is depicted in Figure 1 and comprises three σ, σ^* pairs, the π_{CO}, π^*_{CO} orbital pair, and the two lone pairs of electrons of the oxygen atom. For computational sake, the IQA scheme[10] has been performed using the wave function corresponding to a more modest CASSCF(4,3) method (restricted to the most relevant lone pair of the O and the π, π^* pair of MOs - see Figure 1). The energies of each state are computed state-specific. An analysis of the electronic wavefunctions obtained with the (12,10) and (4,3) active spaces reveals that the main configurations

contributing to the state are the same. In all cases, the basis set employed is the cc-pVTZ.[21] All the geometries and energies were obtained using the MOLCAS 7.8 program.[22]

The Molden2AIM[23] software has been used for the generation of *wfn* files, needed to carry out the QTAIM analysis of the electron density. This analysis has been done through the AIMPAC package of programs,[24] as well as through the PROMOLDEN code,[10] developed by the Quantum Chemistry group of Oviedo University. Additionally, the MULTIWFN software[25] was used to obtain the Laplacian of the ρ function ($\nabla^2\rho$) and the Electron Localization Function (ELF).[26]

3 Results

3.1 Geometries

In order to study the evolution of the S_1 and the T_1 excited states step by step, a total of five geometries, associated with critical points in different potential energy surfaces (PES), have been considered. Figure 2 shows the equilibrium geometry in the electronic ground state S_0 (denoted as *min*S_0) and the optimized S_1 (*min*S_1) and T_1 (*min*T_1) minima. As it can be seen, the optimized S_1 and T_1 minima show pyramidalized C atoms and C−O bonds elongated with respect to the ground state by ca. 0.14 Å. To separate the effect of elongation and pyramidalization, constrained planar optimizations have been also performed in each electronic excited state (*planar*S_1 and *planar*T_1). The latter C_{2v} geometries correspond to structures with an imaginary vibration frequency associated to the loss of planarity. The relative energy of each critical point in each PES is collected in Table 1. As expected the energy of the planar structures is higher than the fully relaxed structures.

3.2 QTAIM analysis in the excited state

To understand which processes are taking place upon excitation, it is illustrative to analyse the charge density separately in: a) the vertical electronic excitation, b) the lengthening of the C−O and c) the C pyramidalization steps.

(a) Vertical transition to the excited state

In Figure 3 the variation of the electron density function, $\Delta\rho(\mathbf{r})$, associated to $S_0 \rightarrow S_1$ excitation process is depicted. The electron density is mainly removed (shown in red) from the

surroundings of the oxygen atom. This depletion is basically equivalent to the $\rho(\mathbf{r})$ associated to a non-bonding orbital. This electron density is then gained (green) by both, the C and O atoms, but there is no electron density between the atoms –fact that can be associated with the idea of populating a π^*_{C-O} MO. As one can see, the analysis of $\Delta\rho(\mathbf{r})$, which is invariant with regard to MO rotations, naturally provides the same understanding about the charge distribution upon excitation, as the MO theory.

Figure 4a shows the reorganization of the atomic electron populations in the vertical excitation. As expected, the most important change takes place in the C−O moiety, where the oxygen transfers 0.293 electrons to the carbon basin.

The electron density can be also expanded in terms of natural MOs χ_i:

$$\rho(\mathbf{r}) = \sum_i n_i |\chi_i(\mathbf{r})|^2 = \sum_{a\in\sigma} n_a |\chi_a(\mathbf{r})|^2 + \sum_{b\in\pi} n_b |\chi_b(\mathbf{r})|^2 \tag{25}$$

where n_i is the occupation number of the natural MO χ_i. As also shown in eq 25, the natural MOs can be grouped according to their symmetry (σ or π) and, consequently, the atomic electron population can be split into σ and π contributions:

$$N^\sigma(\Omega) = \sum_{a\in\sigma} n_a \int_\Omega |\chi_a(\mathbf{r})|^2 d\mathbf{r} \tag{26}$$

$$N^\pi(\Omega) = \sum_{b\in\pi} n_b \int_\Omega |\chi_b(\mathbf{r})|^2 d\mathbf{r} \tag{27}$$

It should be emphasized that N^σ and N^π come from the MO framework and thus they are not physical observables. However, their analysis may still be useful in chemical bonding theory. Moreover, it is interesting to analyze them if we want to find the parallelism between QTAIM results and MO concepts. The σ-π partitioning of the atomic population in the S_0 is shown in Table 2, together with their variations, ΔN, upon vertical excitation. Overall, one "σ electron" is converted into one "π electron" in the electronic excitation. While O loses 0.759 au from its σ distribution, both C and O increase their π electronic population in 0.484 and 0.466, respectively (i.e. larger at the C, as expected from the antibonding character of the MO). This means that around 60% of the oxygen electronic population involved in the electronic transition still belongs to its basin. Similarly, it can be seen that around 40% of the electronic population gained by the C comes from the H atoms, indicating that the transition is not completely described by an $n_O \rightarrow \pi^*_{CO}$ transition.

Also interesting is to follow the change of the electron density and the ellipticity at the bond critical points[7] (Table 3). The $n_O \rightarrow \pi^*$ electronic transition produces an increase of the

electron density in the C basin, implying a larger electronic repulsion with its environment. As a consequence, the electron density at the BCP of the different bonds in which the carbon is involved decreases. Important to note is that although ρ^{BCP} decreases in the three bonds, only the C−O bond distance increases after excitation (see Figure 2), clearly illustrating that the $\Delta\rho^{BCP}$ between two electronic states is not enough to predict the geometric reorganization taking place upon excitation. In passing we note that correlations between ρ^{BCP} and bond length should only be done within the same kind of chemical bonds and an electronic excitation does not assure that bonds in different electronic states share the same chemical nature.

The ellipticity increases in both C−O and C−H bonds, in agreement with the fact that the electron density is accumulated at both sides of the molecular plane over the C atom, implying an electron density distribution along the bonds less cylindrical. This is also a clear example where the association of the ellipticity (or, in general, properties emerging from the electron density) to the bond order (or concepts related to the orbital conception) can be dangerous.

The results of the energy partition following the IQA scheme are collected in Table 4. The first column refers to the change of energies for the vertical excitation. Accordingly, in the S_1 excited state the net energies of C and O decrease whereas the interaction between them, $\Delta V_{int}(C,O)$, becomes very much repulsive (1131 kJ mol^{-1}). As O is negatively charged in the ground state (charge $q_O = -1.118$ au), the withdrawal of electron density from its basins upon excitation stabilizes the atom through the reduction of the electron-electron repulsion in its basin. At the same time, the C in S_0 is positively charged ($q_C = +1.150$ au) and the increment of its atomic electron population increases its nucleus-electron attraction.* However, this redistribution of the electron density also intensifies the electron-electron repulsion between both basins (C−O), destabilizing the interaction between them. It can be also of interest to sum up all the inter-atomic interaction energies depending on $\rho(\mathbf{r})$ in what we call a classical potential, V_{clas}, defined as $V_{int} - V_{xc}$ (recall eqs 21 and 23). The variation of V_{clas} for the CO pair (998.9 kJ mol^{-1}) is pretty close to the one obtained by employing a point-charge model (around 877 kJ mol^{-1}). The same agreement is obtained for the C−H bond (35.1 kJ mol^{-1} *vs ca* 65 kJ

*The variation experienced by $E_{net}(C)$ in this vertical electronic excitation may be basically assigned to a charge transfer term. Thus, ΔE_{net} roughly corresponds to $-IP(C)\cdot\Delta N(C)$, where $IP(C)$ is the ionization potential of the isolated atom. For example, using the IP experimental value for C (11.26 eV), we get an estimated $\Delta E_{net}(C)$ value of -523 kJ mol^{-1}, which satisfactorily compares with our computed value shown in Table 4 (-606 kJ mol^{-1}). This approximation also holds for processes (b) and (c); however, it does not provide good estimations for negatively charged atoms (using electron affinities), where the deformation of the basin plays a more significant role. More details can be found in reference [27].

mol^{-1}). Moreover, an $\Delta V_{xc}(C,O)$ energy of 132.5 kJ mol^{-1} after vertical excitation (see Table S1 in the Electronic Supporting Information (ESI)) indicates that an important part of the double C=O bond breaks. In summary, it can be seen that the stabilization of the individual atoms comprised in the bond and destabilization of the interaction, making the bond strength weaker, is in line with the idea of populating an antibonding MO.

Using the CASSCF(4,3) employed in the IQA scheme, localization and delocalization indices[7] can be obtained (Table 5).[†] In the ground state, the most important differences, comparing the expected values of the ideal Lewis structure for the formaldehyde are found in C and O atoms (λ_C, λ_O, and $\delta_{C,O}$). These differences can be basically justified considering the other resonance form of the C=O bond (C^+-O^-). Upon excitation, the localization indices (λ) follow the total basin electron populations (c.f. Table 2). Since oxygen suffers a loss of electron density, it becomes less prone to share it, decreasing $\delta_{C,O}$. This behavior is again the one expected according to the orbital interpretation because the π^* MO should entail a reduction in the bond order. Indeed, $\delta_{C,O} = 1.098$ au for S_1 is close to the expected value for a single bond. Therefore, the evolution of λ and δ values could be taken as an indication of the partial heterolytic cleavage of the π bond upon vertical electronic excitation. As shown in Table 5, the electrons delocalized in the bond become now localized in one of the two atoms, C.

As it has been previously reported,[28] a change in $\delta_{\Omega,\Omega'}$ accompanying vertical excitation may be used, in general, to predict the evolution of the corresponding bond length. Thus, $\delta_{C,O}$ decreases (-0.199 au) and $\delta_{C,H}$ increases (0.022 au) upon electronic excitation, facts which can be directly related to an stretch and a shrink of the C−O and C−H bonds, respectively (Figure 2).

(b) Lengthening of the C−O bond in the S_1 excited state

After vertical excitation, the nuclei are subjected to new forces and, as a consequence, a geometrical reorganization occurs (in this case the C−O elongates and the C pyramidalizes, see *min*S_1 in Figure 2). In this section we shall analyse energies and populations obtained within the bond elongation only, i.e. at the *planar*S_1 geometry.

The atomic electron population reorganizations that occur in the C−O elongation process are shown in Figure 4b. The oxygen transfers electron density to the C basin (as expected when

[†]The active space used in these calculations introduces correlation basically in the CO moiety, which is the most important one for our purposes. This means, $\delta_{C,O}$ is smaller than the one from Hartree-Fock (HF), while $\delta_{H,H}$ and $\delta_{C,H}$ are very close to those obtained from HF description. Then, the value of 1.297 au for CO is clearly a polarized double bond with correlation, whereas 0.908 au is a single C−H bond without correlation.

the C−O bond is breaking, since at infinite C−O distance O should be neutral). A detailed analysis of the σ and π populations reveals that the nature of the electronic reorganization is practically σ (Table 6). Delocalization indices (Table 5) indicate that, in this process, the C−O bond order is reduced to a value of 0.995 au. Thus, elongation breaks the double bond, homolytically in the π distribution, as no significant changes are observed in π populations, and partially heterolitically in the σ one.

During the C−O elongation process, important changes in the values of ρ^{BCP} and ϵ^{BCP} are not observed, with the exception of the electron density in the C−O, which obviously decreases as a consequence of the C−O cleavage (Table 3).

In the IQA scheme (Table 4) the same trends found in the excitation process are observed: stabilization of C and O net energies and destabilization in their interaction energies. This is again in agreement with the fact that the antibonding character of the π^* MO is responsible of the elongation. However, our analysis indicates that the lengthening of the C−O bond is not accompanied by a transference of the π electron density, but a σ one.

(c) Pyramidalization of the C atom in the S_1 excited state

The electron density reorganization accompanying the pyramidalization (see Figure 4c) is negligible in comparison with the other two processes. Since the total atomic populations remain almost invariable, the localization and delocalization indices (Table 5) as well as the ellipticity and the electron density at the BCPs (Table 3) hardly change. Despite small, it is interesting to note that the variation of the ellipticity at the BCP in the C−O (from 0.162 au at *planar*S_1 to 0.097 at *min*S_1) is associated with a larger σ character, in agreement with the idea that the C atom acquires sp^3-like hybridisation.

The IQA energy partition (Table 4) for pyramidalization does not show any remarkable stabilization. The most important term arises from the C−O interaction, which behaves oppositely as in the excitation and C−O elongation processes. This stabilization, however, is in line with a deformation of the C electron density to reach a sp^3-like hybridisation that occurs to make the bond stronger. In terms of IQA energies this is reflected as a destabilization in E_{net} and a stabilization in V_{int}.

In order to understand why the C pyramidalises, it is useful to look at the terms that define V_{int} (recall eqs 17 and 23) which are contained in Table S3 of the ESI. As it can be seen, the origin of the C−O stabilization is due to the reduction of the electron-electron repulsion between both atomic basins. Thus, the driving force of the pyramidalization seems to be the

reduction of the initial electron-electron repulsion introduced by the vertical excitation (Table S1). This repulsion has its origin (see above) in the π contribution of the electron density (see Figure 3).

For the sake of simplicity, let us consider the ideal spherical out-of-plane π electron densities shown in Figure 5. Taking into consideration only the large interatomic interactions (that is, interactions between spheres in the same side of the plane) depicted as double red arrows, we find that: i) The ρ with π-symmetry in the planar conformation (II) gives rise to $V_{ee}^{\pi} \propto 2nm$ between C and O (being n and m the electronic charge of the spheres); ii) After distortion of the π distribution, transferring certain a and b amounts of electron density (with $a, b \geq 0$) across the plane (as indicated in the imaginary state III), repulsion decreases, since $V_{ee}^{\pi} \propto 2(nm - ab)$;[‡] and iii) Due to the distortion, the local geometric environment of the atoms is modified, causing the pyramidalization of the atom (IV). In plain English, a symmetry-breaking in the electron density reduces the electron-electron repulsion.

In addition, V_{clas} and V_{xc} values for the C−O pair (-71 kJ mol^{-1} and 8.8 kJ mol^{-1}, respectively) indicate that this process is governed by classical energy terms.

3.3 Comparison between S_1 and T_1

In the previous section, an analysis of the changes undergone by formaldehyde after excitation from the S_0 to the S_1 has been done. An alike study can be done for the T_1 state, at the *planar*T_1 and *min*T_1 geometries, and the results obtained are very similar (Table S4).

In Figure 6, the $\Delta\rho(\mathbf{r})$ function between the T_1 and S_1 is shown at *planar*S_1 geometry. The triplet state is characterized by a larger population at the C basin, which has mainly π character (Table 7). This means that the π population of C and O basins are more "alike" in the triplet state than in the singlet one (0.964 and 1.967 au *vs* 1.006 and 1.920 au, for C and O basins, Table 7). According to the mechanism described in Figure 5, larger repulsions between C and O are expected in T_1 and the pyramidalization in the triplet state should be slightly larger. Indeed, the HHOC dihedral angle for *min*S_1 is 22.8 degrees while it is 26.9 degrees for *min*T_1.

Differences in IQA energetic terms (at *planar*S_1 geometry) are all smaller than 5.0 kJ mol^{-1} in absolute value (Table S5), with the exception of the $E_{net}(C)$, whose change is -18.1 kJ mol^{-1}. This is due to the increase in the nucleus-electron attraction in the C basin.

[‡]In this situation, V_{ee}^{π} is proportional to $(n+a)(m-b)+(n-a)(m+b)$.

3.4 Laplacian of the electron density in the excited states

In QTAIM, the Laplacian of the electron density, $\nabla^2\rho(\mathbf{r})$, is typically used to recover the main features of the Lewis and Valence-Shell Electron-Pair Repulsion (VSEPR) models.[29] Similarly, the electron localization function (ELF)[26] is known for its ability to analyze the distribution of electron pairs in the molecule. However, the usual formulation of ELF is only well defined for monodeterminatal wave functions, while $\nabla^2\rho(\mathbf{r})$ can be obtained at any level of theory.

Isosurfaces of the Laplacian of the electron density of S_0 at *min*S_0 and of S_1 at *min*S_0 and *min*S_1 (Figure 7) show two interesting facts. First, upon vertical electronic excitation, the $\nabla^2\rho < 0$ region typically associated to the O lone pairs rotates 90 degrees around the C−O bond. And second, during the pyramidalization, a $\nabla^2\rho < 0$ region (not associated to any bond) appears in the surroundings of the C atom. The isosurfaces of the T_1 at *min*S_0 and *min*T_1 are identical to those of the S_1 and therefore not shown.

In order to visualize the ELF not only in the S_0 but also in the excited state of formaldehyde, we analyzed the T_1, which can be described with one Slater determinant in an unrestricted Hartree-Fock (UHF) formulation. This is in this case justified because the S_1 and T_1 states exhibit similar properties and thus, the ELF analysis may be extended "*mutatis mutandis*" to describe also the S_1. Interestingly, the two facts observed with $\nabla^2\rho(\mathbf{r})$ are also reproduced by the topology of the ELF,[30] as observed in Figure 8.

It is of importance to point that, according to the traditional nomenclature of the $S_0 \rightarrow S_1$ transition ($n \rightarrow \pi^*$), it is expected that the electron density of the lone pairs is transformed into that of a π^* MO. As it is shown here, the topological analysis of ρ (both QTAIM or ELF) enriches this description, showing that this conversion is caused by a rotation of the ρ associated to the O lone pairs, what could be interpreted as that the "σ" lone pairs become "π" lone pairs and this triggers a concomitant weakening of the C−O double bond.

The rotation of the O lone pairs is very relevant, as it appears in a huge number of photophysical processes. It seems reasonable that the O lone pairs are in a σ disposition due to the presence of the C−O double bond in the S_0, even if it maximizes the repulsion between C−H bonding pairs and the O lone pairs. In the S_1 electronic arrangement, the repulsion between the O lone pairs and the C−H bonding pairs is minimized.

4 Conclusions

The main conclusions may be summarized as follows:

- The QTAIM has proved to be versatile enough to be applied to systems in their electronic excited states, generating results that are in line with firmly-established chemical facts and interpretations. Moreover, QTAIM results have not only been as useful as those coming from MOs concepts, but even capable of adding details of electronic rearrangements that are not easily deduced from the MO framework.

- Excitation to the singlet $n\pi^*$ state is accompanied with the stabilization of the individual atoms of the carbonyl bond but with a destabilization of the interaction between them. This fact is in accordance with the idea of populating a π^* MO, being also an indication that the nature of the C−O bond has changed.

- The energy partitions associated to the vertical excitation and to the lengthening of the carbonyl bond show the same trend, that could be also ascribed to the antibonding character of the π^*_{C-O} MO. However, the C−O lengthening does not involve a change in the π contribution of the atomic populations, but in the σ one.

- The pyramidalization of the C atom can be understood as a breaking of the symmetry of the electron density in order to reduce the electron-electron repulsion between C and O basins.

- The analysis of the electron density (through QTAIM and ELF) reveals that the $n \rightarrow \pi^*$ transition may be also understood as a rotation of the oxygen lone pairs to a π disposition, accompanied with a synchronous weakening of the C−O double bond.

5 Acknowledgments

D. F-C. and R. A. M. thank Spanish Ministry of Economy for project CTQ2010-21500. D. F-C. also thanks Spanish Ministry of Education for an FPU fellowship and the University of Vigo for the "Estadía en centros de investigación" grant.

References

[1] M. Klessinger and J. Michl, *Excited States and Photochemistry of Organic Molecules*, VH Publishers, Inc. Toronto, 1995.

[2] F. Weigend, M. Kattannek and R. Ahlrichs, *J. Chem. Phys.*, 2009, **130**, 164106.

[3] L. González, D. Escudero and L. Serrano-Andrés, *Chem. Phys. Chem.*, 2012, **13**, 28–51.

[4] J. Pipek and P. G. Mezey, *J. Chem. Phys.*, 1989, **90**, 4916–4926.

[5] J. M. Foster and S. F. Boys, *Rev. Mod. Phys.*, 1960, **32**, 300–302.

[6] D. A. Kleier, T. A. Halgren, J. H. Hall Jr and W. N. Lipscomb, *J. Chem. Phys.*, 1974, **61**, 3905–3919.

[7] R. F. W. Bader, *Atoms in Molecules: A Quantum Theory*, Oxford: Clarendon Press, 1995.

[8] R. F. W. Bader, *Chem. Rev.*, 1991, **91**, 893–928.

[9] P. L. A. Popelier, *Struc. Bond.*, 2005, **115**, 1–56.

[10] M. A. Blanco, A. M. Pendás and E. Francisco, *J. Chem. Theory Comput.*, 2005, **1**, 1096–1109.

[11] J. Cioslowski, *J. Phys. Chem.*, 1990, **94**, 5496–5498.

[12] P. Mori-Sanchez, J. Recio, B. Silvi, C. Sousa, A. M. Pendas, V. Luaña and F. Illas, *Phys. Rev. B*, 2002, **66**, 075103.

[13] R. F. W. Bader, D. Bayles and G. L. Heard, *J. Chem. Phys.*, 2000, **112**, 10095.

[14] Y.-G. Wang, K. B. Wiberg and N. H. Werstiuk, *J. Phys. Chem. A*, 2007, **111**, 3592.

[15] P. B. Coto, D. Roca-Sanjuán, L. Serrano-Andrés, A. M. Pendás, S. Martí and J. Andrés, *J. Chem. Theory Comput.*, 2009, **5**, 3032.

[16] R. Chávez-Calvillo and J. Hernández-Trujillo, *J. Phys. Chem. A*, 2011, **115**, 13036–13044.

[17] V. Tognetti and L. Joubert, *Chem. Phys. Lett.*, 2013, **557**, 150–153.

[18] N. J. Turro, *Modern molecular photochemistry*, Menlo Park, California: The Benjamin Cummings, 1978.

[19] C. F. Matta and R. J. Boyd, *The Quantum Theory of Atoms in Molecules: From Solids State to DNA and Drug Design*, Wiley-VCH, 2007.

[20] B. O. Roos, P. R. Taylor and P. E. M. Siegbahn, *Chem. Phys.*, 1980, **48**, 157–173.

[21] T. H. Dunning, *J. Chem. Phys.*, 1989, **90**, 1007–1023.

[22] F. Aquilante, L. De Vico, N. Ferré, G. Ghigo, P. Malmqvist, P. Neogrády, T. B. Pedersen, M. Pitoňák, M. Reiher, B. O. Roos, L. Serrano-Andrés, M. Urban, V. Veryazov and R. Lindh, *J. Comput. Chem.*, 2010, **31**, 224–247.

[23] *Zou, W., Molden2AIM, http://people.smu.edu/wzou/program/index.html*.

[24] R. Biegler-Knig, R. Bader and T.-H. Tang, *J. Comput. Chem.*, 1982, **13**, 317.

[25] T. Lu and F. Chen, *J. Comput. Chem.*, 2012, **33**, 580 – 592.

[26] A. D. Becke and K. E. Edgecombe, *J. Chem. Phys.*, 1990, **92**, 5397–5403.

[27] A. M. Pendás, M. A. Blanco and E. Francisco, *J. Comput. Chem.*, 2006, **28**, 161–184.

[28] A. M. Pendás, M. Blanco and E. Francisco, *J. Comput. Chem.*, 2009, **30**, 98–109.

[29] R. J. Gillespie and P. L. A. Popelier, *Chemical Bonding and Molecular Geometry*, Oxford University Press, 2001.

[30] I. Fourré, B. Silvi, P. Chaquin and A. Sevin, *J. Comput. Chem.*, 1999, **20**, 897–910.

Table 1: Relative energies (eV) of formaldehyde obtained at the CASSCF(12,10)/cc-pVTZ level of theory.

	S_0	S_1	T_1
minS_0	0.00[a]	4.52	4.26
planarS_1	0.66	4.00	3.79
minS_1	1.07	3.94	3.67
planarT_1	0.58	4.01	3.78
minT_1	1.12	3.96	3.66

[a]Energy of -114.04552 au

Table 2: Atomic populations for the S_0 state (total as well as σ and π components) and their change after the vertical $S_0 \rightarrow S_1$ electronic excitation. All values are in au and referred to the *min*S_0 geometry.

	N_{S_0}	$N^{\sigma}_{S_0}$	$N^{\pi}_{S_0}$	ΔN	ΔN^{σ}	ΔN^{π}
C	4.850	4.365	0.484	0.489	0.006	0.484
O	9.118	7.629	1.489	-0.293	-0.759	0.466
H1/H2	1.016	1.001	0.015	-0.098	-0.122	0.023
$\sum$	*16.000*	*13.997*	*2.003*	*0.000*	*-0.996*	*0.996*

Table 3: Electron density ρ (au) and ellipticity ϵ at the bond critical point (BCP) of C−O and C−H bonds. The absolute values refer to the S_0 state at the *min*S_0 geometry while variations are calculated for (a) the vertical excitation $S_0 \rightarrow S_1$, (b) the C−O elongation, and (c) the C pyramidalization.

			(a)		(b)		(c)	
	$\rho^{BCP}_{S_0}$	$\epsilon^{BCP}_{S_0}$	$\Delta\rho^{BCP}$	$\Delta\epsilon^{BCP}$	$\Delta\rho^{BCP}$	$\Delta\epsilon^{BCP}$	$\Delta\rho^{BCP}$	$\Delta\epsilon^{BCP}$
C−O	0.41953	0.124	-0.01196	0.015	-0.10505	0.023	0.00227	-0.064
C−H	0.28318	0.021	-0.02414	0.067	0.01912	-0.004	-0.00239	-0.030

Table 4: Changes in the intra-atomic net energies and the inter-atomic interaction energies (kJ mol^{-1}) for the processes (a), (b), and (c) considered in Figure 4. The data correspond to the CASSCF(4,3)/cc-pVTZ level of calculation.

	(a)	(b)	(c)
ΔE_{net}(C)	-606.0	-290.2	57.8
ΔE_{net}(O)	-203.1	-398.4	10.5
ΔE_{net}(H1)[a]	37.7	-9.7	-10.1
ΔV_{int}(C,O)	1131.4	654.5	-62.2
ΔV_{int}(C,H1)[a]	36.8	-32.0	-5.9
ΔV_{int}(O,H1)[a]	-43.8	28.1	11.8
ΔV_{int}(H1,H2)	16.1	0.0	-6.6

[a]The same as H1 for H2.

Table 5: Expected values for the localization (λ, diagonal values) and the delocalization (δ) indices for the Lewis standard structure of formaldehyde at S_0, the calculated values for S_0 at *min*S_0 geometry, and the change of these indices for the $S_0 \rightarrow S_1$ excitation, C−O elongation and C pyramidalization. All the values are in au and calculated at the CASSCF(4,3)/cc-pVTZ level of theory.

	λ_Ω & $\delta_{\Omega,\Omega'}$	C	O	H1	H2
S_0 Lewis	C	4.000			
	O	2.000	7.000		
	H1	1.000	0.000	0.500	
	H2	1.000	0.000	0.000	0.500
S_0 at *min*S_0	C	3.305			
	O	1.297	8.389		
	H1	0.908	0.112	0.458	
	H2	0.908	0.112	0.051	0.458
$S_0 \rightarrow S_1$ at *min*S_0	C	0.559			
	O	-0.199	-0.222		
	H1	0.022	0.007	-0.088	
	H2	0.022	0.007	-0.019	-0.088
min$S_0 \rightarrow$ *planar*S_1 in the S_1 state	C	0.147			
	O	-0.103	-0.033		
	H1	0.029	-0.036	0.001	
	H2	0.029	-0.036	0.000	0.001
planar$S_1 \rightarrow$ *min*S_1 in the S_1 state	C	-0.064			
	O	-0.016	0.006		
	H1	-0.006	0.010	0.032	
	H2	-0.006	0.010	0.002	0.032

Table 6: Atomic populations for the S_1 state (total as well as σ and π components) at the *min*S_0 geometry and their change in the C−O elongation. All values are in au.

	N_{S_1}	$N^{\sigma}_{S_1}$	$N^{\pi}_{S_1}$	ΔN	ΔN^{σ}	ΔN^{π}
C	5.339	4.371	0.968	0.170	0.174	-0.004
O	8.826	6.871	1.955	-0.179	-0.190	0.011
H1/H2	0.918	0.880	0.038	0.004	0.008	-0.004
$\sum$	*16.000*	*13.001*	*2.999*	*0.000*	*0.000*	*0.000*

Table 7: Atomic populations for S_1 and T_1 (total as well as σ and π components) at the *planar*S_1 geometry and their difference (T_1 minus S_1). All values are in au.

	N_{S_1}	$N^{\sigma}_{S_1}$	$N^{\pi}_{S_1}$	N_{T_1}	$N^{\sigma}_{T_1}$	$N^{\pi}_{T_1}$	ΔN	ΔN^{σ}	ΔN^{π}
C	5.509	4.545	0.964	5.556	4.551	1.006	0.048	0.005	0.042
O	8.647	6.680	1.967	8.617	6.697	1.920	-0.030	0.017	-0.047
H1/H2	0.922	0.888	0.035	0.913	0.877	0.037	-0.009	-0.011	0.002
$\sum$	*16.000*	*13.001*	*2.999*	*16.000*	*13.001*	*2.999*			

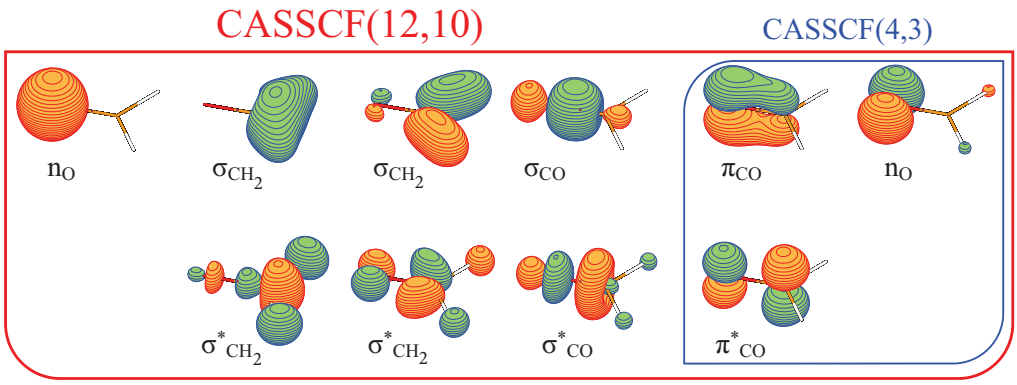

Figure 1: Natural molecular orbitals of formaldehyde included in the CASSCF(12,10) active space; here, exemplary for the S_0 state. The subset selected for the subsequent CASSCF(4,3) single point calculations is in the blue box.

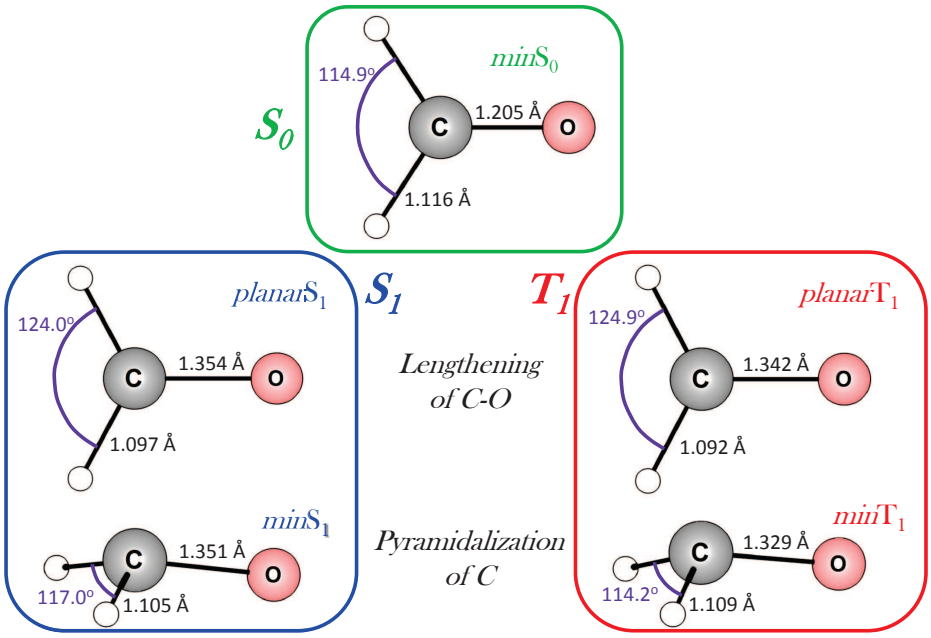

Figure 2: Equilibrium geometries of formaldehyde in the S_0, S_1 and T_1 electronic states, as well as planar structures in the S_1 and T_1 excited states. Bond distances in Å and H−C−H angle in degrees.

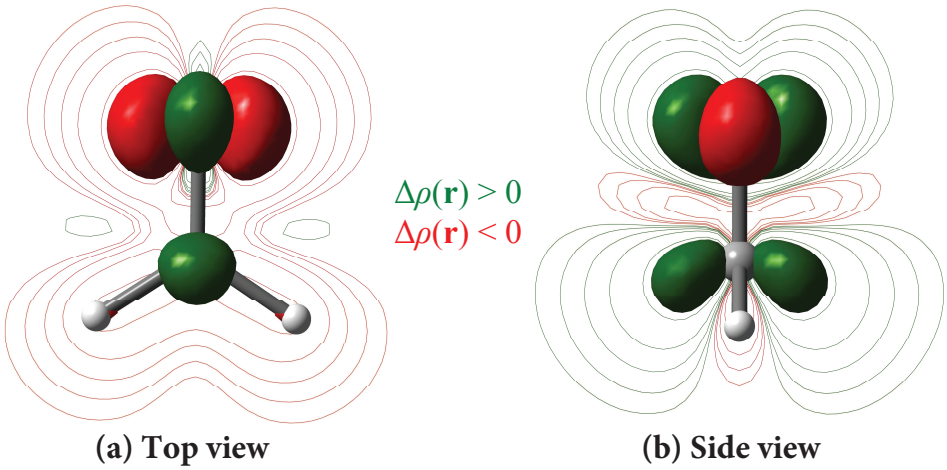

Figure 3: (a) Top view and (b) side view of the electron density variation, $\Delta\rho(\mathbf{r})$, in the vertical electronic excitation $S_0 \rightarrow S_1$. Isosurfaces of ± 0.025 au and isolines of ± 0.001, ± 0.002, ± 0.004, ± 0.008, and ± 0.020 au are shown (positive in green, negative in red).

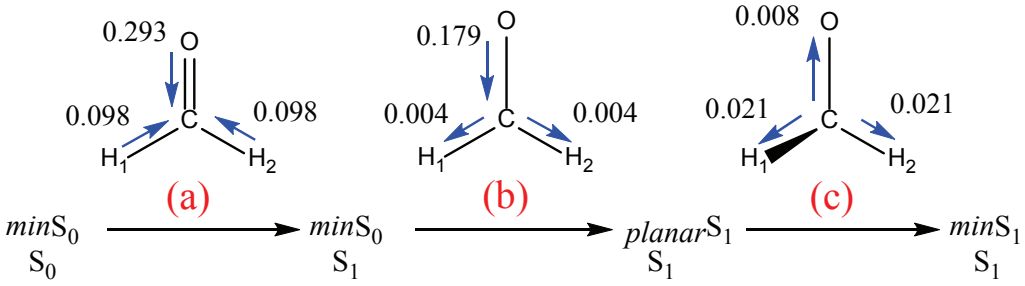

Figure 4: Reorganization of the electron density (au) from *min*S_0 (in S_0 state) to *min*S_1 (in S_1) in (a) the vertical electronic excitation $S_0 \rightarrow S_1$ in the *min*S_0 geometry, (b) the lengthening of the C−O bond in the excited state, and (c) the pyramidalization of the carbonyl carbon.

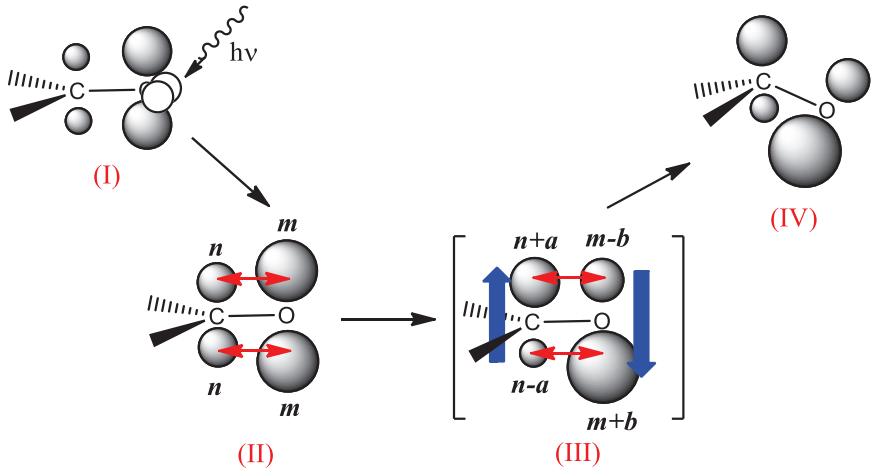

Figure 5: Scheme of the pyramidalization of the carbonyl carbon. This process takes place in order to reduce the repulsion between the out-of-plane electron densities at C and O.

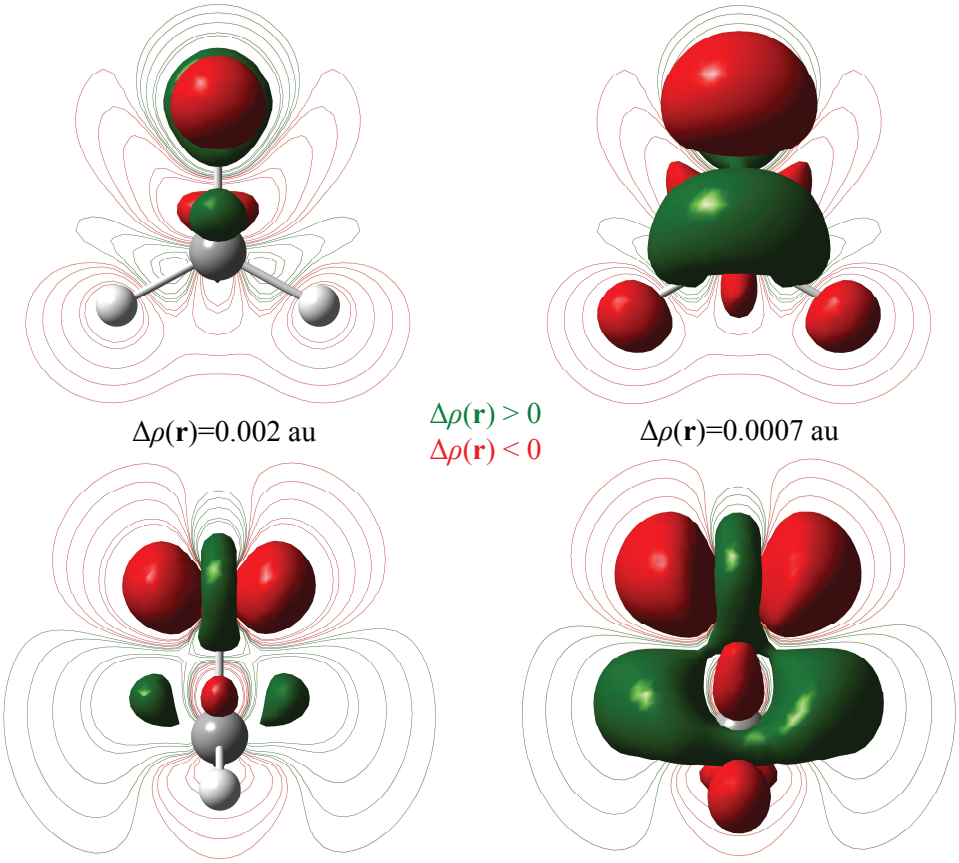

Figure 6: $\rho_{T_1} - \rho_{S_1}$ at the *planar*S_1 geometry. Isosurfaces of ± 0.002 and ± 0.0007 au and isolines of ± 0.0001, ± 0.0002, ± 0.0004, ± 0.0008, and ± 0.001 au are shown (positive in green, negative in red.)

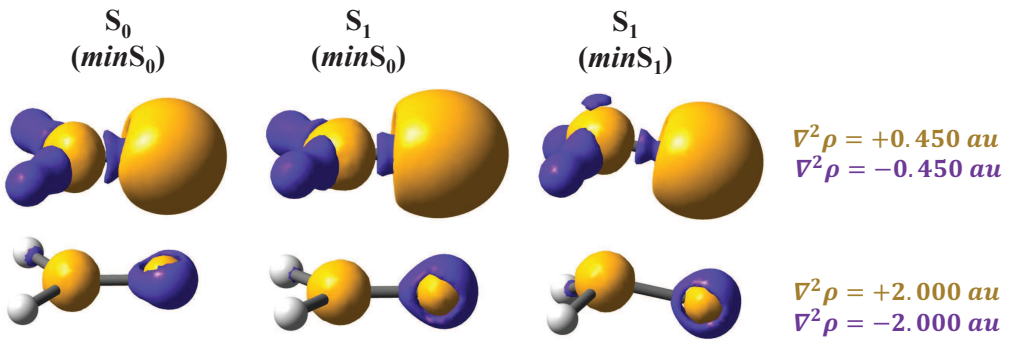

Figure 7: $\nabla^2\rho$ isosurfaces ($\pm$0.4 au and $\pm$2.0 au; positive in yellow, negative in violet) obtained from the electron density of the S_0 (at *min*S_0) and S_1 (at *min*S_0 and *min*S_1) states. The electron density was obtained at a CASSCF(12,10)/cc-pVTZ level of theory.

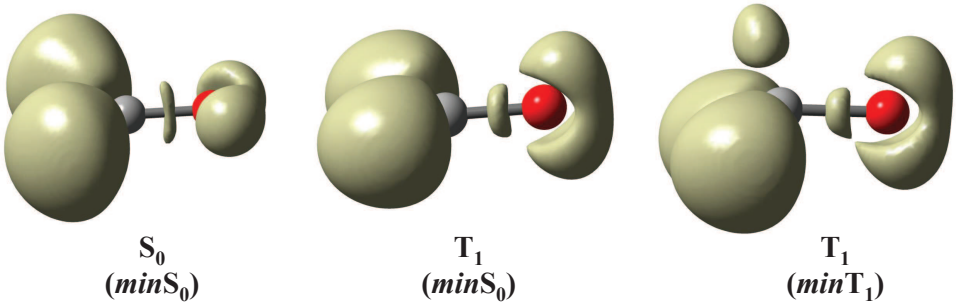

Figure 8: 0.85 au ELF isosurface for the the S_0 (at *min*S_0) and T_1 (at *min*S_0 and *min*T_1) states. The ELF was obtained at the UHF/cc-pVTZ level of theory.